Design and optimisation of electrically propelled blended-wing body aircraft

Perret Du Cray, J., Bolam, R.C. and Vagapov, Y.

Design and Optimisation of Electrically Propelled Blended-Wing Body Aircraft

Josephine Perret du Cray
Wrexham University
Wrexham, UK

Robert Cameron Bolam
Wrexham University
Wrexham, UK

Yuriy Vagapov
Wrexham University
Wrexham, UK

***Abstract*—This paper presents the study and design of an electrically powered blended-wing body aircraft and assesses the viability and performance of the blended-wing body airframe combined with electric engine propulsion, aiming to identify a functional and efficient ecological solution. The focus is on the implementation of an electrically driven rim fan as the propulsion system for the test aircraft. Based on the requirements for a test aircraft, a preliminary design is established, and several blended-wing body test aircraft models are proposed and modelled using numerical design tools. These concepts are then subjected to fluid dynamics and stability simulations using ANSYS Fluent. The geometry with the best results is ultimately selected and optimised. The project results in a blended-wing body test aircraft that meets the design specifications and successfully integrates the electrically driven rim fan into the airframe while maintaining the high aerodynamic performance characteristic. The final aircraft achieves a lift-to-drag ratio of 16.47, representing an improvement of nearly 20% compared to the flying wing designs represented in the literature review.**

Keywords—BWB, aircraft electrical propulsion, rim driven fan, UAV

I. Introduction

Today's combustion engines are mainly responsible for the emission of polluting particles, with a ratio of 2 kg of CO2 released for one litre of fuel [1]. Fortunately, there are already some credible solutions to this problem: such as hybrid, hydrogen or biofuel engines, synthetic aviation fuel, solar engines or electric engines. Major companies such as Airbus are now looking at biofuels and hydrogen [2],[3]. However, these solutions do not provide 100% carbon reduction, unlike battery electric propulsion. Unlike biofuels, pure electrical propulsion also provides partial noise reduction and total NOx reduction [4].

In addition to research into the cleanest possible propulsion, alternative airframe configurations are also being studied with the aim of optimising aircraft performance by replacing traditional aircraft designs. These investigations will make it possible to envisage the future of aeronautics in the medium to long term (2030-2050) without being too extensive in terms of development costs and resources [5],[6]. The ideas under consideration include distributed propulsion and boundary layer ingestion (BLI) and also involve a total redesign of the airframe with concepts such as ground effect vehicles (GEVs) [7] or Blended-Wing Body (BWB) aircraft.

Blended-Wing Body (BWB) aircraft are one of the most promising concepts for green aviation because of their environmentally sustainable potential. This is mainly due to highly aerodynamic characteristics such as its low generated drag and high lift. However, in some respects, this configuration does not yet meet all the criteria of viability (stability, flight control, passenger comfort) nor all the non-pollution targets, and is therefore still a contestable solution.

This paper presents a study and design of an electrically powered BWB and considers the viability and performance of the BWB airframe in an electric engine propulsion combination to find a functional and efficient ecological solution. The intended electrical powerplant is named the Fast-Fan (FF) and is an innovative electrical rim-driven fan being developed by Wrexham University [8]-[11].

Based on the requirements for an electrically powered test aircraft, a preliminary design is established, and several BWB test aircraft models are proposed and modelled using design tools. These concepts are then subjected to fluid and stability simulations (using ANSYS Fluent and Solidworks). The geometry with the best results is finally selected and optimised.

II. Electrical Propulsion System

The electrical propulsion system comprises of a 440 VDC Lithium-ion battery pack which enables a fifteen-minute flight duration for the test aircraft whilst allowing a good operational safety margin. Earlier studies conducted at Wrexham University indicated that a standard flight-test circuit would only require a flight time under five minutes [11]. To ensure safe and efficient operation, an onboard battery management system (BMS) and SiC inverters (electronic speed controllers) are included in the electrical system, to balance the current whilst charging and discharging, and to control the supply frequency and the speed of the two rim-driven motors respectively.

To enable thrust and balance symmetry, it is intended that the test aircraft will have one FF propulsor device installed on the aircraft centreline. The FF is a dual rotor

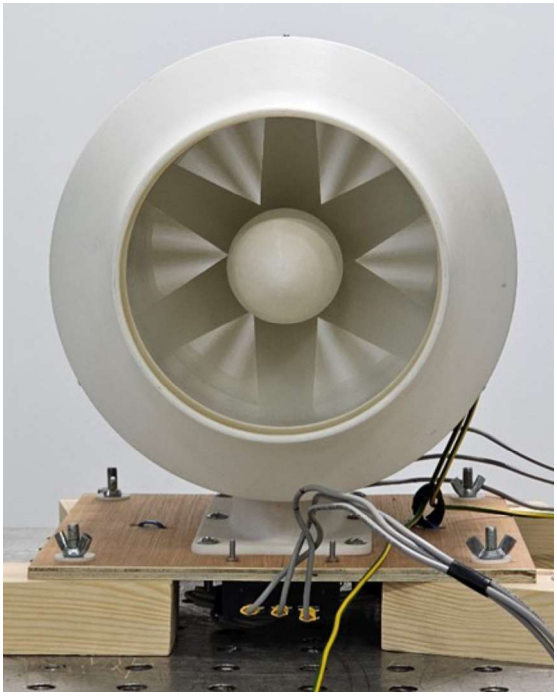

Fig. 1. Prototype Fast-Fan device, viewed on the exhaust nozzle, whilst undergoing laboratory testing.

979-8-3315-6520-6/25/$31.00 ©2025 IEEE

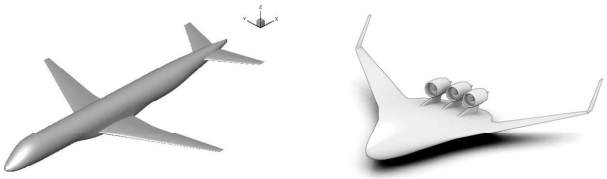

(a) (b)

Fig. 2. Comparison of examples of TAW (a) and BWB (b) geometries.

contrarotating ducted fan, and the rotors are housed in a low -drag, aerodynamically shaped cowling resembling a podded turbo-fan engine with a pitot-type intake and a jet-pump type exhaust nozzle. Fig. 1. shows a prototype FF device, viewed on the exhaust nozzle, whilst undergoing laboratory testing. This view clearly shows the interference pattern produced by the movement of the counterrotating fans and the stationary six-vaned central structural support.

Each FF has two AC synchronous permanent magnet motors with independently controlled, twelve-pole, three-phase motor windings. The FF has an overall efficiency of 80% which includes the electrical inverter and motor efficiencies and the isentropic efficiencies of the fans. The maximum design speed of the rotors is 15,000 RPM, and the power rating of the FF is 30 kW. Because of the extra leverage provided by the rim drive configurations and the supply voltage level, the peak winding currents are maintained at a modest 35 A. The electrical stator windings are housed within the duct and cooled by the passage of ambient air drawn over the windings by the jet-pump action of the exhaust airflow.

Flight control of the aircraft will be possible in manual and automatic modes. In the manual mode, the aircraft will be controlled by means of a pilot-held, radio-controlled handset. In the automatic mode, global navigation satellite systems (GNSS) and a laptop ground station will be configured to guide the aircraft using pre-programmed mission software and telemetry hardware. .

III. Blended-Wing Body Geometry

The development of BWB begins with the development of flying wings. Pure flying wings were first investigated by Reimar and Walter Horten in Germany, and by Jack Northrop in the USA, between 1935 and 1940 [12]. This wider-than-long body, with no fuselage or tail to minimise weight and drag, enabled these pioneers to establish remarkable flight performance for the time, especially in terms of speed and endurance; however, one of the main concerns was the sizing of the control surfaces needed to counteract the stability problems. The technology of the time did not allow for complete stability laws to be obtained or solved [13].

Thanks to the evolution of computing power and onboard systems, the Northrop company was later able to develop the American B-2 stealth bomber, which is still in use today. As these flying wing models evolved, the appearance of a fuselage was necessary in order to house the cockpit, landing gears, weapons bay, etc. The aircraft engineer Vincent Burnelli was a pioneer in this field and designed a structure where the aerofoil-shaped fuselage could contribute 30% of the lift [14].

From this concept the BWB was finally born, a flying wing with centre section blended into delta wing panels without distinct horizontal and vertical stabilizers, by contrast with the established tube and wing (TAW) aircraft. The TAW configuration is defined as a cylinder fuselage providing volume, horizontal and vertical tails realizing stability and a wing generating lift. Quantitative comparisons between the conventional TAW body and BWB have been extensively studied highlighting the unusual characteristics of the latter. A comparison of TAW and BWB geometries is illustrated in Fig. 2.

Thus, although the TAW model is used by all the major manufacturers today, reducing shape drag by decreasing the wetted surface area, made the BWB stand out. This shape also increases spanwise efficiency through the use of a lifting fuselage and reduces interference drag by smoothly merging wings and body. Furthermore, this junction improves manufacturability, structural efficiency and high aerodynamic efficiency in flight [15].

Raymer [12] offers a lot of information on all types of aircraft but does not deal in depth with the BWB. However, the profile of the flying wing is well studied there, and the relationship between these two models allows for obtaining the following results, which will be used for the rest of the study: aspect ratio is 3; taper ratio (λ) is 0.2; quarter chord sweep angle is 57°; lift/drag ratio (L/D) max is 16.

Panagiotou et al. [7] study a medium-altitude-long-endurance (MALE) BWB UAV, whose dimensions and mission profile are similar to those of this study. The issue of weight is addressed here and introduces the notions of gross take-off weight (GTOW) W_0, payload weight W_p, fuel weight W_f and empty weight W_e, linked by the following relationship: $W_0 = W_p + W_f + W_e$.

In the case of electric propulsion, the weight of the fuel does not exist and the GTOW therefore only consists of the payload weight (camera, recovery chute), and the empty aircraft weight, i.e. the weight of the structure, engine, batteries and avionics. Furthermore, unlike fuel weight, which decreases as fuel is consumed during the flight, the weight of the batteries remains constant, which greatly simplifies weight estimation and sizing calculations.

IV. Electrical Design Requirements

The Fast-Fan is an experimental sub-scale podded electric engine with a ducted fan and features an innovative winding configuration, making it particularly small and light for power output. It is 500 mm long, with a diameter of 300 mm, weighs a maximum of 15 kg, and is capable of delivering 300 N of thrust. This motor is powered by lithium-ion batteries, which have a very high-power density, which means a high-power output for a low weight, thus a very interesting property when it comes to aviation. In order to supply the 440 V needed to power the engine, 120 batteries will be used, for a total mass of about 14 kg.

The aircraft itself will be a test aircraft, designed to monitor the behaviour of the engine in flight and to assess its compatibility with a very likely future BWB configuration. Its flight time will be 5 min. The anticipated flight profile of the sub-scale demonstrator will therefore be very simple: (1) warm-up, (2) take-off, (3) cruising and loitering, (4) descent and then (5) landing.

The desired dimensions are approximately 4 m wingspan, for a maximum mass of 50 kg. Its take-off speed will be 65 m/s; in the rest of the study, this will also be considered its cruising speed. In addition to the essential equipment needed to fly the aircraft (engine, batteries, controller, electronic speed control ESC, etc.), some elements are desired on the aircraft, such as a recovery chute, a camera and an undercarriage.

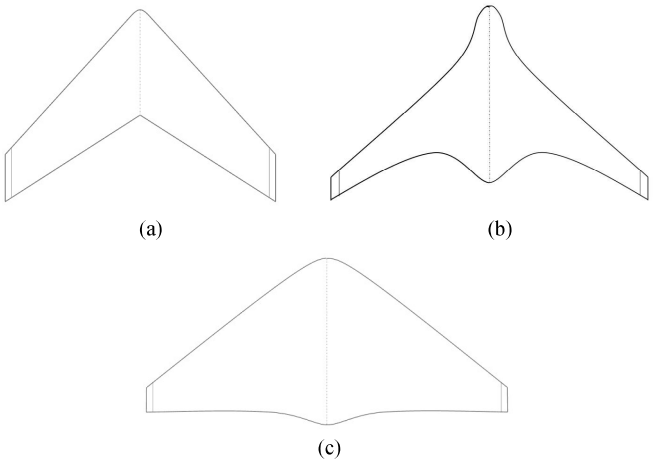

Fig. 3. (a) PARROT configuration, (b) NASA configuration, (c) QUEST configuration.

V. BWB Aircraft Designs

A. Tailless Aircraft Designs

The first idea is to take and adapt a flying wing developed in 2016 by the drone company Parrot, so it will be referred to in the study as the "PARROT" configuration. As shown in Fig. 3a, this is an airframe with a simple geometry and is known for its simplicity in flight. The second model is a more complex geometry with curved shapes, inspired by the BWB commercial aircraft concept developed by NASA in the 2000s, the BWB-450 [14],[16], so it will be referred to in the study as the "NASA" configuration (Fig. 3b). The latest design, shown in Fig. 3c, stems directly from a draft idea presented at the beginning of the FF project as a BWB test aircraft: the QUEST (Quick Electrical System Test) aircraft [10],[11].

B. Tail Aircraft Designs

The absence of a tail in the BWB configuration is both an advantage and a disadvantage. A study will therefore be carried out on profiles with a small horizontal tail, in order to evaluate its impact on the longitudinal stability of the profile but also its aerodynamic performance.

The first model with a tail (Fig. 4a) is a model based on the manta shape of the X-48 prototype built by NASA, with the tail widened to achieve a real effect on stability. Indeed, the X-48 proved itself in flight but required too much active stabilisation [17]. It will be called for the continuation of the project the "MANTA" configuration.

However, since only one FF engine is planned for the test aircraft, the MANTA configuration with a single tail may have a disadvantage depending on the position of the engine. Indeed, if the FF is placed in the middle aft of the airframe, the airflow could be disturbed around this single tail and render it ineffective. A dual tail configuration is therefore also considered, illustrated in Fig. 4b. It will be referred to in the study as the "SWALLOW" configuration.

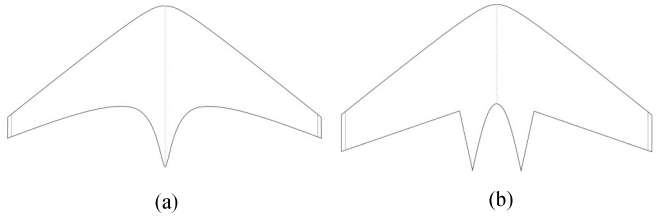

Fig. 4. (a) MANTA configuration, (b) SWALLOW configuration.

VI. Analysis Methodology

Once the designs were chosen, the models were created and modified in 3D, so that they could then be subjected to numerical simulations and their performance evaluated. This modelling process takes place initially on OpenVSP, also known as Open Vehicle Sketch Pad. This is an open-source parametric tool for aircraft geometry, originally developed by NASA in the early 1990s. The software allows for the rapid generation of models from ideas, especially unconventional geometries, making it a tool of choice for the project.

Furthermore, in addition to the CFD and FEA (Finite Element Analysis) analyses available, OpenVSP also has modules for aerodynamic analysis of the models, some of which will be useful in the rest of the study including:

- Mass Properties Analysis – to compute properties like centre of gravity and moment of inertia.
- Projected Area Analysis – to compute project area.
- VSPAero – for vortex lattice or panel method-based aerodynamic and flight dynamic analysis.

A. Ranking of Profiles by Numerical Fluidic Simulations

With the 3D models obtained, the first numerical simulations were performed. The first step was to determine the appropriate domain and mesh size so that the CFD calculations performed would converge, whilst being as fast, accurate and computationally efficient as possible. The results allowed the models to be ranked according to their aerodynamic behaviour and to select two of the best-performing models. The domain study, meshing, and CFD process are conducted using modules from the ANSYS Workbench 2021 R2 system, developed by ANSYS, Inc.

B. Domain Dependency Studies

When studying a profile subjected to fluid motion, CFD calculations are not performed on the geometry itself, but rather on the fluid surrounding it. Thus, before starting any simulation steps, it is necessary to create a box representing the air around the test aircraft model to optimise the calculation time. However, the size of this box must be chosen with care. It must be large enough not to disturb the flow near the domain limits (to preserve the free flow stream), which would make the simulation diverge and thus distort the results. It must however remain of a reasonable size, in order to optimise the calculation time. Using Ansys Design Modeller a sketch is drawn around the model in three characteristic dimensions H1, H2 and V3, and extruded along D1. Each design has a different geometry, so they will all have a different size domain. The process of defining the size of the box is therefore carried out individually for each design (Table I). In order to save computational time, this and all subsequent studies will be carried out on half a profile.

Using the Boolean operator, the 3D model is then subtracted from the box and the fluidic domain is ready. The box is now meshed with ANSYS Meshing; edge sizing and

Table I. Ideal Domain Dimensions for Each Design

Model Configuration	H1 (m)	H2 (m)	V3 (m)	D1 (m)
PARROT	11	17.6	19.8	11
NASA	29.6	40.7	19.8	29.6
QUEST	11	17.6	19.8	11
MANTA	31.14	41.52	19.8	31.14
SWALLOW	22.4	32	19.8	22.4

TABLE II. IDEAL MESH DEFINITION FOR EACH DESIGN

Model Configuration	Global mesh (m)	Face sizing mesh (m)	Edge sizing mesh (m)	Number of elements
PARROT	1	0.1	0.183	1,018,152
NASA	1	0.1	0.02	1,373,694
QUEST	0.8	0.08	0.015	1,158,230
MANTA	0.8	0.065	0.01	1,038,360
SWALLOW	0.7	0.05	0.007	1,521,217

face sizing are applied, in addition to a 1m element size mesh. It is essential to keep the same mesh for all boxes so that only the size of the domain influences the final results.

C. Mesh Dependency Studies

Like the domain dependency study, the mesh dependency study allows for finding the optimal mesh applied to the studied profile. The characteristic feature of this investigation is the number of elements in the mesh, ranging, for the same design, from a linear mesh of 200,000 elements to a linear mesh of 2,000,000 elements. For each design, approximately 6 meshes are built on ANSYS Meshing, consisting of a global mesh, a face size and an edge size. Respectively, these mesh elements vary in size from 2 m to 0.45 m, 0.6 m to 0.05 m and the edge sizing 0.075 m to 0.0045 m. These meshes are then tested using the same numerical simulation as in the domain study, and the results are obtained as the L/D ratio. When this ratio is related to the size of the mesh, a zone of convergence can be seen, allowing the suitable mesh to be defined for each design (Table II).

D. Ansys Fluent Simulation Setup

Once the optimal domains and meshes have been defined for each design, the simulations for ranking the aerodynamic performance can be run. The work done in the previous sections ensures the reliability of the results and allows a comparison between all the designs. The vast majority of fluidic simulations applying to BWB aircraft geometries are based on RANS equations, where all turbulence effects are modelled. In ANSYS Fluent, the k-epsilon and k-omega incompressible viscous models belong to the RANS family. They are two-equation models and are semi-analytical, which makes them interesting because they are economical to run and close to reality. The standard k-omega is used for small Reynolds numbers (below 500,000) and offers superior performance for complex boundary layer flows under adverse pressure gradients and separations,

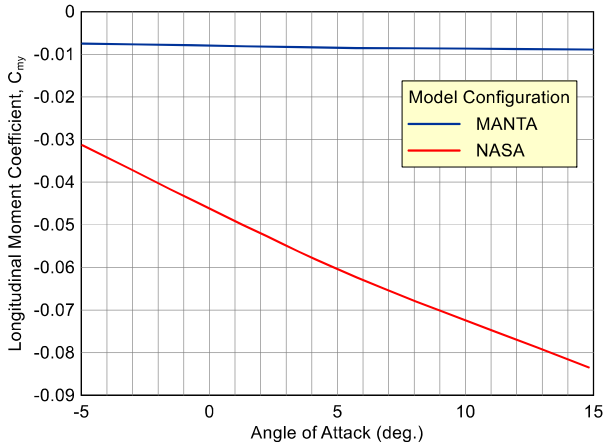

Fig. 5. Longitudinal moment coefficient C_{my} as a function of the angle of attack for MANTA and NASA configurations.

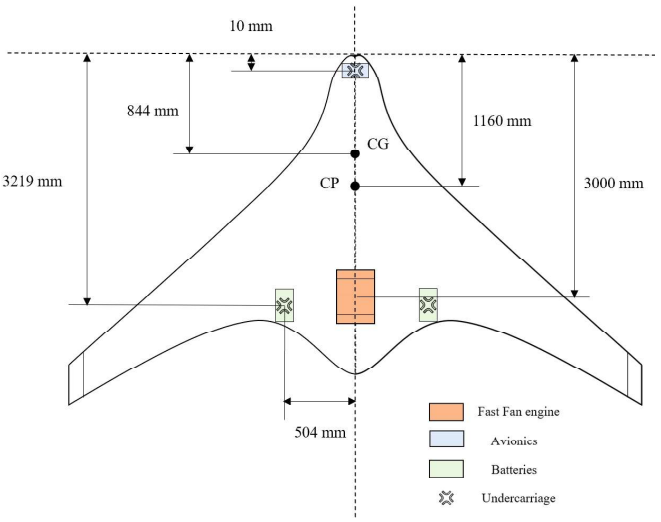

Fig. 6. Diagram of the final configuration of the BWB NASA test aircraft.

such as for external aerodynamics studies. The *k*-omega model is therefore the most suitable for this study and has been used for both dependency studies and applied for all CFD simulations.

The inlet air velocity is the one given by the specification, while its density and viscosity are calculated using standard formulas.

$$\rho = \frac{p}{RT} \tag{1}$$

where ρ is the air density, p is the air pressure, R is the ideal gas constant, T is the air temperature $T = 15°C$ ($T_0 = 288.15$ K) at the altitude $h = 100$ m above sea level.

$$p = p_0\left(1 - \frac{Lh}{T_0}\right)^{\frac{gM}{RL}} \tag{2}$$

where p_0 is the sea level standard pressure (101325 Pa), L is the temperature lapse rate (0.0065 K/m), T_0 is the sea level standard temperature (288.15 K), g is the gravitational acceleration (9.81 m/s²).

Viscosity is defined as follows $\mu = 2.791\times10^{-7}\times T^{0.7355}$.

E. Ansys Fluent Simulation Results

The values found allowed the five BWB test aircraft ideas to be modelled consistently. The results are the respective lift and drag coefficients for all configurations, with the L/D ratio as the overall comparison. The values are collected in Table III.

Numerical simulations were run on ANSYS. Like the first CFDs, a box is created on ANSYS Modeler, with the same dimensions as those obtained during the domain dependency study of the NASA configuration. The adapted

TABLE III. CFD SIMULATION RESULTS

Model Configuration	Coefficient of Lift C_l	Coefficient of Drag C_d	Lift-to-drag Ratio L/D
PARROT	0.1943	0.0119	16.3277
NASA	0.3287	0.0184	17.8544
QUEST	0.1897	0.01	18.97
MANTA	0.1925	0.0124	15.5242
SWALLOW	0.2813	0.0193	14.5751

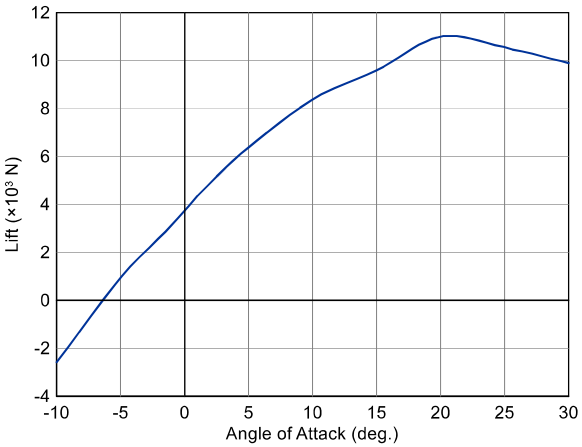

Fig. 7. Lift generated by the NASA aircraft at each angle of attack.

mesh is then applied to it in ANSYS Meshing before naming the surfaces for further processing.

In order to perform well, the test aircraft must have a lift coefficient of at least 0.13, a coefficient of drag below 0.078 and an L/D ratio of more than 13.86. As shown in Table III, each of these designs meets these criteria. However, the FF engine is not yet integrated into the fuselage. When it is, the airflow will be disturbed, and a large amount of drag will be produced. Thus, the SWALLOW configuration is discarded due to its low L/D ratio; with the addition of the duct, the L/D ratio will fall below 13.86, jeopardising the viability of the completed concept. The other L/D ratios are correct. To optimise the study, the best of the tailless designs and the best of the tail designs are selected. The NASA and MANTA configurations are therefore used in the study. Therefore, the handling characteristics, aerodynamics and structure of the aircraft will be preserved throughout the flight.

F. Stability Study

The stability study of the NASA and MANTA configurations performed in Solidworks gives the moments of inertia presented in Table IV. According to these data, these two models are the most unstable not longitudinally but laterally, in roll (I_{xx}). It is interesting to note that the addition of the tail, despite the expected leverage effect, neither improves nor worsens the resistance to pitch motion, characterized by I_{zz} under Solidworks. So, the pitch moment must be managed by a short moment arm and not a long one.

The graph shown in Fig. 5 is the longitudinal moment coefficient (about the Y-axis in OpenVSP) related to the angle of attack of the NASA and MANTA test aircraft.

It is known that longitudinal static stability is achieved when for a positive disturbance, the aircraft must naturally produce a negative moment opposing the movement. Conversely, when the disturbance is negative, the moment must be positive. In other words, when the angle of attack is negative, C_{my} is positive. As the AoA increases, the longitudinal moment coefficient decreases; at a certain angle of attack, ideally 0°, C_{my} is 0. Thus, when no disturbance causes the aircraft to deviate from its trajectory, no motion correction is induced. When the AoA is greater than 0°, C_{my} becomes negative [17].

TABLE IV. MOMENTS OF INERTIA

Inertia	**Model Configuration**	
	NASA	MANTA
I_{xx} (km×m^2)	40.06	20.8
I_{yy} (km×m^2)	296.72	97.29
I_{zz} (km×m^2)	333.78	115.15

As can be seen in Fig. 5, none of the configurations exhibit this behaviour, indicating that none of them fulfils the criterion of longitudinal stability. Nevertheless, it can be observed that the NASA configuration lends itself more easily to modifications leading to the ideal behaviour since its curve tends to meet the AoA = 0° axis more quickly than that of the MANTA profile. The difference in the behaviour of the two configurations as reflected in the difference in their curves can also be further investigated in future research.

This first stability analysis allows the selection of the NASA geometry for the continuation and conclusion of the study. Fig. 6 summarises the final BWB test aircraft configuration following the placement of all elements according to the results obtained during this stability study.

Once the model has been finalised, it is important to verify its viability and maintain it in all flight states, i.e. at all angles of attack from 0° to 30°.

The stall curve resulting from the parametric study is presented in Fig. 7. It can be seen that from about +20° the lift generated by the aircraft slowly decreases. This is a soft stall; still, the aircraft should avoid pitch angles greater than 20°. However, BWB aircraft generally take off at an angle of 14-15° [14], which is below the stalling region, so the aircraft can take off safely.

VII. CONCLUSION

The results obtained from this study have made it possible to design and select a BWB test aircraft configuration from several proposals, to optimise it, evaluate it and analyse possibilities for future integrations (BLI and distributed propulsion).

The outcome is a model that meets the specifications provided in terms of weight, dimensions, context of use and the requirements linked to the BWB nature of the aircraft (reflex airfoil and angle of departure). In addition, the aerodynamic performance of the aircraft is better than that calculated during the preliminary design: the NASA geometry generates 1.5 times more lift and 7 times less drag than predicted. An improvement of almost 20% in the L/D ratio is observed compared to the flying wings presented in the literature review. This result can be further improved by investigating issues such as optimising stagnation points, particularly at the front of the aircraft, and better integration of the engine with the airframe.

However, there remains a major deficiency with this test aircraft; the instability of the model makes the NASA configuration unviable and therefore not usable at this time. This problem, intrinsically linked to the tailless nature of BWBs, has been consistently encountered in papers on the subject.

Nevertheless, while for commercial applications this is still a problem, there are many functional UAV flying wings or BWBs available today. A more in-depth study of stability by design will probably have to be carried out, as well as analyses to determine the sizing coefficients of the control surfaces. For a small model, flight-by-wire can be envisaged without it being too heavy and too expensive [16],[18],[19].

References

[1] A. Wangai, S. Kiinzhikeyev, J. Rohács, and D. Rohacs, "Comparison of total lifecycle emission of aircraft with different propulsion system," *Aeronautical Science Bulletins*, vol. 29, no. 3, pp. 337–348, Dec. 2017.

[2] Airbus and TotalEnergies sign strategic partnership for sustainable aviation fuels. [Online]. Available: https://www.airbus.com/en/newsroom/press-releases/2024-02-airbus-and-totalenergies-sign-strategic-partnership-for-sustainable

[3] Airbus. ZEROe: our hydrogen-powered aircraft. [Online]. Available: https://www.airbus.com/en/innovation/energy-transition/hydrogen/zeroe-our-hydrogen-powered-aircraft

[4] Environmental Research and Consultancy Department, "Emerging Aircraft Technologies and their potential noise impacts," Civil Aviation Authority, West Sussex, 2019.

[5] Y. Ma and A. Elham, "Designing high aspect ratio wings: A review of concepts and approaches," *Progress in Aerospace Sciences*, vol. 145, 2024, Art. no. 100983, doi: 10.1016/j.paerosci.2024.100983

[6] I. Abrantes, A.F. Ferreira, L.B. Magalhaes, M. Costa, and A. Silva, "The impact of revolutionary aircraft designs on global aviation emissions," *Renewable Energy*, vol. 223, 2024, Art. no. 119937, doi: 10.1016/j.renene.2024.119937

[7] C. Papadopoulos, D. Mitridis, K. Yakinthos, "Conceptual design of a novel unmanned ground effect vehicle (UGEV) and flow control integration study," *Drones*, vol. 6, no. 1, 2022, Art. no. 25, doi: 10.3390/drones6010025

[8] R.C. Bolam and Y. Vagapov, "Implementation of electrical rim driven fan technology to small unmanned aircraft," in *Proc. 7th Int. Conf. on Internet Technologies and Applications ITA-17*, Wrexham, UK, 12-15 Sep. 2017, pp. 35–40, doi: 10.1109/ITECHA.2017.8101907

[9] R.C. Bolam, Y. Vagapov, R.J. Day, and A. Anuchin, "Aerodynamic analysis and design of a rim driven fan for fast flight," *Journal of Propulsion and Power*, vol. 37, no. 2, pp. 179–191, Mar. 2021, doi: 10.2514/1.B37736

[10] R.C. Bolam, J.P.C. Roque, Y. Vagapov, and A. Dianov, "Prototype testing of rim driven fan technology for high-speed aircraft electrical propulsion," in *Proc. 59th Int. Universities Power Engineering Conf. UPEC*, Cardiff, UK, 2–6 Sep. 2024, pp. 1–5, doi: 10.1109/UPEC61344.2024.10892569

[11] R.C. Bolam, J.P.C. Roque, Y. Vagapov, R.J. Day, and M. Slepchenkov, "A power budget analysis of an electrical uncrewed air vehicle (UAV) flying a basic mission profile," in *Proc. 58th Int. Universities Power Engineering Conf. UPEC*, Dublin, Ireland, 30 Aug. – 1 Sep. 2023, pp. 1–5, doi: 10.1109/UPEC57427.2023.10294620

[12] D.P. Raymer, *Aircraft Design: A Conceptual Approach*, 6 ed., Playa del Rey, California: AIAA, 2018, p. 838.

[13] R.L. Schwader, "The development of the flying wing," *Journal of Aviation/Aerospace Education and Research*, vol. 8, no. 4, pp. 7-13, 1997, doi: 10.58940/2329-258X.1212

[14] Z. Chen, "Assessment on critical technologies for conceptual design of blended-wing-body civil aircraft," *Chinese Journal of Aeronautics*, vol. 32, no. 8, pp. 1797-1827, Aug. 2019, doi: 10.1016/j.cja.2019.06.006

[15] M.-F. Liou, H. Kim, B.J. Lee, and M.-S. Liou "Aerodynamic design of integrated propulsion-airframe configuration of the hybrid wingbody aircraft," in *Proc. 35th AIAA Applied Aerodynamics Conference*, Denver, USA, 5-9 June 2017, Art. no. 3411, doi: 10.2514/6.2017-3411

[16] NASA, *Beyond Tube-and-Wing*, Washington DC: NASA Aeronautics Book Series, 2020.

[17] T.S. Sugandi, Nathan, S.K. Subrata, O. Arifianto, and M.A. Moelyadi, "Prediction of static stability in tandem wing unmanned aerial vehicle," *Journal of Physics: Conference Series*, vol. 1130, 2018, Art. no. 012028, doi: 10.1088/1742-6596/1130/1/012028

[18] Y.O. Aktas, U. Ozdemir, Y. Dereli, A.F. Tarhan, A. Cetin, and A. Vuruskan "A low cost prototyping approach for design analysis and flight testing of the TURAC VTOL UAV," in *Proc. Int. Conf. on Unmanned Aircraft Systems (ICUAS)*, Orlando, FL, USA, 27-30 May 2014, pp. 1029-1039, doi: 10.1109/ICUAS.2014.6842354

[19] A. Mohamed, K. Massey, S. Watkins, and R. Clothier, "The attitude control of fixed-wing MAVS in turbulent environments," *Progress in Aerospace Sciences*, vol. 66, pp. 37-48, 2014, doi: 10.1016/j.paerosci.2013.12.003